Mining, Metallurgy & Exploration (2020) 37:129–139
https://doi.org/10.1007/s42461-019-00135-2

Numerical Investigation of the Effect of a Novel Wet Scrubber on Dust Reduction in an Underground Coal Mine

Sampurna Arya[1] · Thomas Novak[2]

Received: 24 January 2019 / Accepted: 3 September 2019 / Published online: 16 September 2019

Abstract
Controlling dust generation and keeping it below permissible limits to meet federal dust standards at the working face of a room-and-pillar coal mine is a challenge for a mine operator. With the recent changes in federal dust regulations requiring lower worker exposure, maintaining compliance has become increasingly difficult. The current most effective practice of dust control at a continuous miner face in an underground mine is the use of a flooded-bed scrubber. A study carried out by the National Institute for Occupational Safety and Health (NIOSH) indicated that a flooded-bed scrubber could achieve cleaning efficiencies between 58 and 90%. But, the operation of such a system is maintenance intensive. The flooded-bed scrubber screen becomes clogged with dust particles and requires frequent cleaning to maintain performance. However, the dust control issue is not solely a mining industry problem. Other industries face similar issues. The University of Kentucky collaborated with Toyota Motor Manufacturing on the development of a novel wet scrubber, called the vortecone scrubber, for capturing oversprayed paint particles in automotive paint booths. The vortecone scrubber achieved a cleaning efficiency of 99% and required minimal maintenance. This study aims to assess the ability of this vortecone scrubber to capture respirable dust in an underground coal mine. The paper presents the results of computational fluid dynamics (CFD) modeling of this vortecone scrubber. It discusses the effects of air quantity and dust particle size on the performance of the scrubber.

Keywords Dust control · Dust scrubber · Flooded-bed scrubber · Respirable dust · Room-and-pillar mine · Computational fluid dynamics (CFD)

1 Introduction

Dust generation at the face of an underground coal mine is an unavoidable phenomenon. No matter the practices employed, it inevitably occurs as a by-product of coal extraction and coal transportation. The effect of dust has had a significant impact on the health of mining personnel. Prolonged exposure to airborne respirable dust (dust particles of aerodynamic diameter < 10 μm) can cause coal workers' pneumoconiosis (CWP), silicosis, emphysema, and chronic bronchitis, collectively known as black lung [1]. Black lung, an incurable disease, results in a buildup of inhaled dust in the lungs that can be neither destroyed nor removed from the body and causes lung damage, permanent disability, and death [2]. The severity of the disease increases with the length of exposure, its intensity, and size of inhaled particles. According to NIOSH, black lung killed more than 10,000 miners between 1995 and 2004 [3].

In addition to being a health issue, coal dust is also a safety issue for underground coal miners. The generated dust, if not captured at its generation point, is dispersed into the mine atmosphere through the ventilating air and deposited downwind on the return entries' surfaces. In the event of a methane explosion, the coal dust, if insufficiently diluted with rock dust, triggers a catastrophic secondary coal dust explosion resulting in more damage to life and property [4]. The Jim Walters No. 5 Mine and the Upper Big Branch Mine disasters, which together killed 42 people and resulted in damage worth millions of dollars in property, are recent examples of coal dust explosions [5, 6].

The first major step taken against black lung was the enactment of the Federal Coal Mine Health and Safety Act of

✉ Sampurna Arya
sampurna.arya@gmail.com; snarya@alaska.edu

Thomas Novak
thomas.novak@uky.edu

[1] Department of Mining & Geological Engineering, University of Alaska Fairbanks, 1760 Tanana Loop, 305 Duckering, Fairbanks, AK 99775, USA

[2] Department of Mining Engineering, University of Kentucky, Lexington, KY, USA

1969 in the aftermath of the Farmington mine disaster. The act provided many protections for coal miners, including dust exposure limits and a workers' health surveillance program. It required each underground coal mine to maintain respirable dust limits at or below 2.0 mg/m^3 in an active working area and 1.0 mg/m^3 in the intake entries. The enactment of this act resulted in a decrease in the prevalence of CWP for underground coal miners. However, after a continued period of decline in CWP from 1970 to 1995, a rising trend from 1995 to 2006 prompted the federal government to promulgate more stringent dust regulations (Fig. 1) [3]. Consequently, in 2009, the Mine Safety and Health Administration (MSHA) launched the "End Black Lung - ACT NOW" campaign to tackle black lung through rulemaking, enhanced enforcement, collaborative outreach, education, and training [7]. Subsequently, in 2010, MSHA proposed a new dust standard to improve underground miners' health protection by lowering their exposure to respirable coal dust [8]. The new dust standard was put into effect on August 1, 2014 and fully implemented on August 1, 2016. It mandated the reduction of the average dust level at the working face to 1.5 mg/m^3 and in intake entries to 0.5 mg/m^3 [9]. After the implementation of the new dust rule, it has become quite challenging for mine operators to meet the permissible dust level requirements using the same dust control techniques previously employed without interrupting production. Therefore, there is a need to improve dust control techniques.

The most popular dust control techniques in an underground mine include dilution through ventilation air, suppression by water sprays, and dust capture through a machine-mounted wet scrubber [10–15]. In the USA, a flooded-bed scrubber is used as an integral part of a continuous miner unit to capture and remove the airborne dust generated at a room-and-pillar mine face (see Fig. 2). The flooded-bed scrubber works on the principle in which water is sprayed to create a large number of water droplets, and the dust-laden air is made to pass through it. In this process, as dust particles come in contact with water droplets, they become captured in the water droplets and are separated from the air.

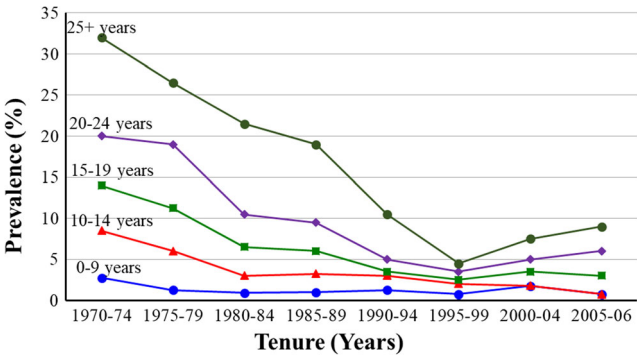

Fig. 1 CWP prevalence among examinees employed at U.S. underground coal mines

The flooded-bed scrubber was invented by Dr. John Campbell in 1983 [16]. It has six main components: an inlet, which is strategically placed adjacent to the cutting drum to capture the maximum possible amount of dust from the face; a full cone water spray, which typically sprays 0.4 L/s (6.5 gpm) water at 310 kPa (45 psi) on the flooded bed to make it wet; a wire-mesh screen downwind of the spray; a demister downwind of the flooded bed; a water sump under the demister; and a vane axial exhaust fan at the outlet. The exhaust fan creates a negative pressure, which draws the dust-laden air from the working face into the scrubber's inlet. The dust-laden air then passes through the flooded bed (a wire-mesh screen), where the dust particles get entrained in the water droplets. The dust-laden water droplets move downwind from the flooded bed to the demister. The demister, which consists of parallel sinuous layers of metal plates, separates the dust-laden water droplets from the air before the air reaches the fan. The dirty, dust-laden water flows down to the sump, where it is pumped out and discharged via the continuous miner's discharge conveyor. The clean, dry air passes through the fan and goes to the return.

The flooded bed is placed at an angle of approximately 45° from the duct floor to maximize the surface area. It consists of 10 to 30 layers of woven, 89-μm steel-mesh screen. The greater the number of layers, the better the performance and the higher the pressure drop across the flooded bed. The fan sizes typically range from 9.7 kW (13 hp) to 29.8 kW (40 hp), with an airflow range from 1.7 m^3/s (3.5 kcfm) to 4.7 m^3/s (10 kcfm) [17].

There are two metrics used to evaluate the performance of a wet scrubber—namely capturing efficiency and cleaning efficiency. Capturing efficiency is the percentage of the generated dust that is captured by the scrubber, and cleaning efficiency is the percentage of dust removed from the captured dust-laden air [18]. A study conducted by NIOSH found that a flooded-bed scrubber, under optimum conditions, can achieve a cleaning efficiency of 90% [19]. Another recent study on the performance of a flooded-bed scrubber shows a reduction of respirable dust concentration by 91%, 86%, and 40% in three different mines A, B, and C, respectively [20, 21]. A relatively lower reduction in the case of mine C was attributed to that mine's adverse geologic conditions, which resulted in a collection of fewer samples and a large deviation in data.

Although the flooded-bed scrubber has been successful in removing dust from a room-and-pillar mine face, its cleaning efficiency and maintenance requirements are still in question. The wire-mesh screen becomes clogged with dust particles, reducing airflow through the scrubber, and therefore requires frequent cleaning to maintain performance. In 2011, a study indicated that a flooded-bed scrubber with a 20-layer wire-mesh screen lost between 20 and 35% of scrubber airflow after every 12.2 m (40 ft) cut in a deep-cut mining practice [22]. In a recent study, previously mentioned in this section, it was observed that after every 6.1 m (20 ft) cut, a flooded-bed scrubber with a 30-layer screen lost 29% and 35% of airflow

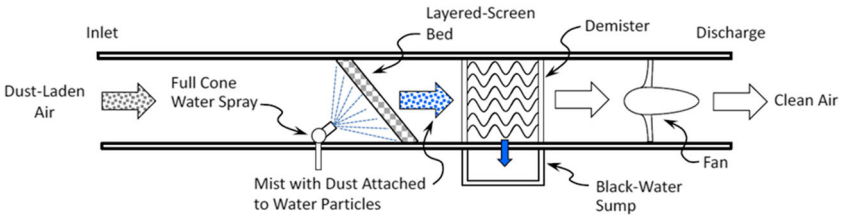

Fig. 2 Cross-sectional view of a flooded-bed dust scrubber

in mines B and C, respectively [20, 21]. From these results, we can see that continuous miner scrubbers require improvements in cleaning efficiency and maintenance frequency.

The research presented in this paper explores the possibility of replacing the maintenance-intensive flooded-bed scrubber with a maintenance-free vortecone scrubber, discussed in Section 1.1. The vortecone scrubber has been tested in other industrial settings and is expected to have higher efficiency and lower maintenance requirements in comparison with flooded-bed scrubbers.

1.1 The Novel Vortecone Scrubber

The vortecone scrubber was invented by a group of researchers led by Dr. Kozo Saito and Dr. Abraham J. Salazar at the University of Kentucky, U.S., in 2000 [23]. It was developed in collaboration with Toyota Motor Manufacturing for capturing oversprayed paint particles in automotive paint booths, and it is currently being used in seven Toyota assembly plants in the USA and Japan [24]. It is a tried and tested technology that has already proven its usefulness in industrial settings. Figure 3 shows a 3-D computer-aided design (CAD) model of the vortecone.

The vortecone scrubber works on the principle of vortex interaction of the particle-laden airflow with water for its particle-capturing mechanism. Particle-laden air enters at the inlet and flows through the vortecone. Water is injected at the periphery of the inlet, creating a water film that circulates on the inner wall of the vortecone. When a particle encounters the water, it becomes entrained in the circulating water. As shown in Fig. 4, the vortecone has four main components: a cone-shaped inlet, a mixing chamber, a vortex chamber, and a discharge. The cone-shaped inlet provides smooth acceleration of particle-laden air and the water film. This acceleration increases the momentum of the particles in the air, which hit a pool of water in the mixing chamber, where some particles are trapped. Particle-laden air then moves to the vortex chamber. The vortex chamber creates a swirling flow of air, imparting a centrifugal force to the particles, pushing them outward. This causes particle-water interaction at the wall of the vortecone. Finally, clean air and dirty water leave the vortecone through its discharge. One of the main reasons for the effectiveness of the vortecone scrubber is the extended resident time of particles in the capturing device. The resident time increases the opportunity for and frequency of collisions between particles and water, and thereby improves performance [24].

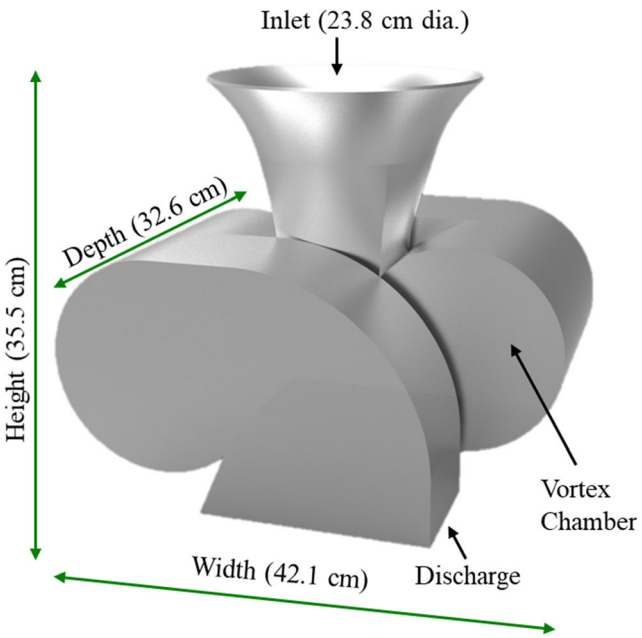

Fig. 3 A 3-D model of the vortecone scrubber

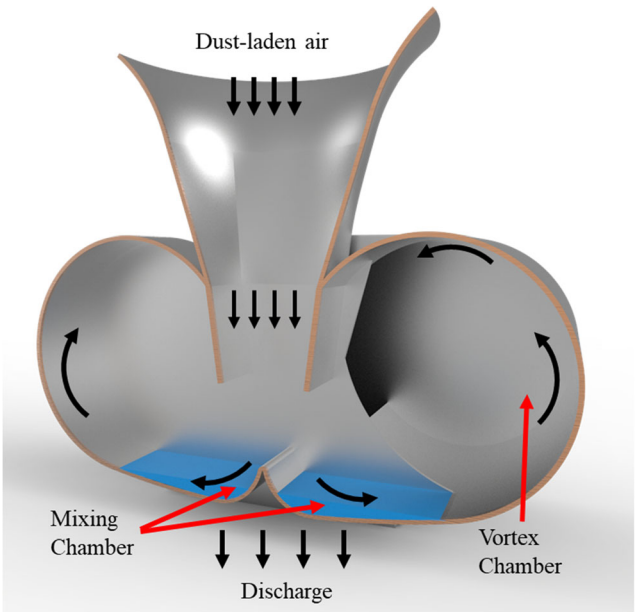

Fig. 4 A cross-sectional view of the vortecone scrubber

The potential advantage of using the vortecone wet scrubber over the flooded-bed scrubber lies in its high cleaning efficiency. Research conducted at the University of Kentucky to capture oversprayed paint particles indicated that a vortecone wet scrubber can achieve a cleaning efficiency of 99.6%, which is much higher than the maximum cleaning efficiency of a flooded-bed scrubber (~ 90%) [19]. In addition, the results of a feasibility study performed to evaluate the application of vortecone scrubber technology in capturing coal combustion fly ash particulate matter, of size 10 μm or less, showed an average cleaning efficiency of 99.8% [25]. Another potential benefit of using the vortecone scrubber concerns maintenance. Because a vortecone scrubber is free of components that can clog, it requires less maintenance, ensuring that dust capture always remains at a high level.

2 Computational Fluid Dynamics Modeling

Computational fluid dynamics (CFD) modeling is a tool for numerically solving complex fluid flow and heat transfer problems. This technique is also used to understand, predict, and analyze fluid dynamics phenomena for analyzing the performance of a design. Kurnia et al. [26] investigated various methods used for mitigating dust dispersion at a mine face and concluded that the application of a brattice offered best results. Yueze et al. [27] studied methane and dust dispersion at a room-and-pillar mine face. Geng et al. [28] utilized numerical technique to investigate dust dispersion driven by a hybrid ventilation system in an underground coal roadway and examined the effects of various parameters on dust dispersion characteristics throughout the coal roadway. Gilmore et al. [29] developed a meshing technique to study bleeder-ventilated gob in a longwall mine. Hu et al. [30] performed a numerical simulation of gas-solid two-phase flow in a coal roadway after blasting and verified the simulation results using field data. Lolon et al. [31] performed CFD simulation on the longwall gob breathing. Wang et al. [32] examined ventilation airflow characteristics at a longwall face for different shearer position and cutting sequences. Similar to the previous research, Zhou et al. [33] studied the diffusion behavior of respirable dust at the longwall mine face and proposed a comprehensive system for dust control. Fig et al. [34] investigated methane ignition and flame propagation in cylindrical tubes to study methane-driven longwall coal mine explosions and established an empirical relationship between tube size and methane-air flame burning velocity. Ajayi et al. [35] studied the effectiveness of radon control measures in cave mines.

This study used the CFD technique to investigate the capability of the novel vortecone scrubber to capture dust. The commercial CFD package Cradle SC/Tetra V12, which is used for thermo-fluid analysis, was employed. A 3-D model of the vortecone was created using a CAD package, PTC Creo, from data presented in United States patent US 6,024,796 (see Fig. 3).

A total of five cases for different vortecone inlet velocities were studied for this research: 6.0, 8.0, 10.0, 12.0, and 14.0 m/s. The five cases were selected considering the variation in inlet velocity with scrubber system resistance and scrubber fan speed. Each simulation was performed in two steps: (a) a single-phase, steady-state simulation was conducted to establish airflow in the computational domain, representing conditions before dust release and (b) a multiphase, transient-state simulation that involved the transport and tracking of solid particles was performed for dust captured by the vortecone, representing the state after dust release. The air was considered as the continuous phase, whereas dust particles were treated as a discrete phase. All the simulations were performed with double precision on a Linux workstation having four 12 core, 2.4 GHz, AMD processors, and 128-GB memory.

2.1 Governing Equations

The working fluid (air) was assumed to be incompressible. Mass, momentum, and energy conservation equations for an incompressible fluid can be written as follows [36]:

$$\frac{\partial u_i}{\partial x_i} = 0 \tag{1}$$

$$\frac{\partial \rho u_i}{\partial t} + \frac{\partial u_j \partial u_i}{\partial x_j} = -\frac{\partial p}{\partial x_i} + \frac{\partial}{\partial x_j}\mu\left(\frac{\partial u_i}{\partial x_j} + \frac{\partial u_j}{\partial x_i}\right) - \rho g_i \beta (T - T_0) \tag{2}$$

$$\frac{\partial \rho C_P T}{\partial t} + \frac{\partial u_j \rho C_P T}{\partial x_j} = \frac{\partial}{\partial x_j} K \frac{\partial T}{\partial x_j} + \dot{q} \tag{3}$$

where u_i is the flow velocity in m/s in x_i direction, t is the time in seconds, ρ is the density in m^3/s, P is the fluid pressure in Pa, μ is the viscosity in Pa s, g_i is the gravity in m/s^2, β is the coefficient of volume expansion in K^{-1}, T is the fluid temperature in K, T_0 is the reference fluid temperature in K, C_P is the specific heat at constant pressure in J/(kg K), K is the thermal conductivity in W/(m K), and $\dot{q}$ is the heat source in W/m^2.

2.2 Turbulence Model

A study was performed on five turbulence models (standard k-ε, RNG k-ε, MP k-ε, realizable k-ε, and Spalart-Allmaras) to see the effects of the different models on simulation results. The test condition with 12.0-m/s scrubber inlet velocity was selected, and simulation results were compared for the steady-state scenario. The magnitude of average air velocities was measured and compared at the ten points shown in Fig. 5. An analysis of results indicated a maximum deviation among the five turbulence models of 3.8% from their mean velocity (Fig. 6).

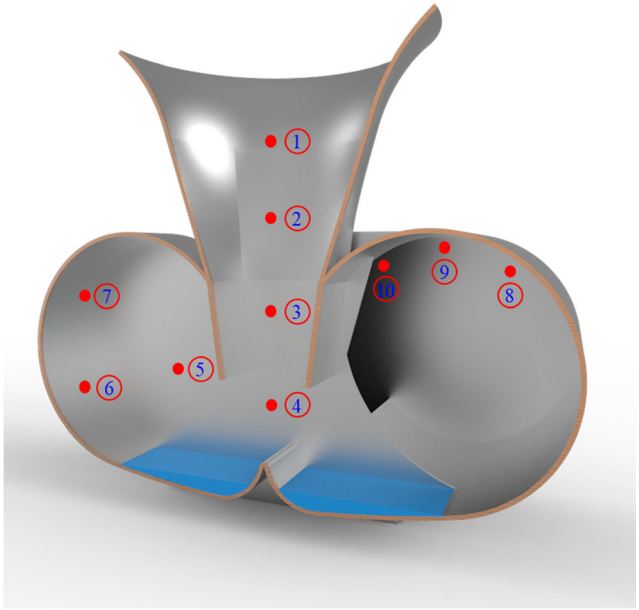

Fig. 5 Locations of the points of average velocity measurement for turbulence model comparison and mesh independence study

Based on the above findings, the most commonly used and well-validated turbulence model in engineering, the standard k-ε turbulence model, was chosen for this study. The standard k-ε turbulence model is a two-equation model that solves the following two separate transport equations for turbulent kinetic energy, k, and specific dissipation rate, ε:

$$\frac{\partial \rho k}{\partial t}+\frac{\partial \rho k u_i}{\partial x_i}=\frac{\partial}{\partial x_j}\left[\left(\mu+\frac{\mu_t}{\sigma_k}\right)\frac{\partial k}{\partial x_j}\right]+G_k+G_b-\rho\varepsilon \quad (4)$$

$$\frac{\partial \rho \varepsilon}{\partial t}+\frac{\partial \rho \varepsilon u_i}{\partial x_i}=\frac{\partial}{\partial x_j}\left[\left(\mu+\frac{\mu_t}{\sigma_\varepsilon}\right)\frac{\partial \varepsilon}{\partial x_j}\right]+C_{1\varepsilon}\frac{\varepsilon}{k}(G_k+G_{3\varepsilon}G_b)-C_{2\varepsilon}\frac{\rho\varepsilon^2}{k} \quad (5)$$

where k is the turbulent energy in m^2/s^2, ε is the turbulent dissipation rate in m^2/s^3, G_k is the generation of turbulent kinetic energy that arises due to mean velocity gradient, G_b is the generation of turbulent kinetic energy that arises due to buoyancy, and σ_k and σ_ε are turbulent Prandtl numbers for the turbulent kinetic energy and its specific dissipation rate, respectively. The eddy viscosity, μ_t, is given by

$$\mu_t=\rho C_\mu\frac{k^2}{\varepsilon} \quad (6)$$

where σ_k, σ_ε, $C_{1\varepsilon}$, $C_{2\varepsilon}$, $C_{3\varepsilon}$, and C_μ are empirical constants and their values are 1.0, 1.3, 1.44, 1.92, 0.0, and 0.09, respectively.

2.3 Discrete Phase Model

The behavior of dust particles was simulated using the particle-tracking feature of Cradle SC/Tetra. Particle tracking uses the Lagrangian equation of conservation to track the trajectory of particles or clusters of particles through the computational domain [36]. The Lagrangian approach treats the air as a continuum fluid and dust particles as discrete particles in fluid space, and the motion of a particle in the airflow is determined by Newton's second law of motion, written as

$$\text{Rate of change of momentum of a particle} = F_g + F_D \quad (7)$$

where F_g and F_D are the body force by gravity and drag force by fluid, respectively. A particle is assumed to be a sphere negligibly small compared with the volume of a fluid in a control volume. For the body force, volume V_p and mass M_p of a particle are calculated by the following equations:

$$V_p=\frac{1}{6}\pi D_p^3 \quad (8)$$

$$M_p=\rho_p V_p \quad (9)$$

where D_p and ρ_p are the diameter and density of a particle, respectively. The drag force from the fluid was calculated by the following formula:

$$F_D=C_D\frac{1}{2}\rho V^2 A \quad (10)$$

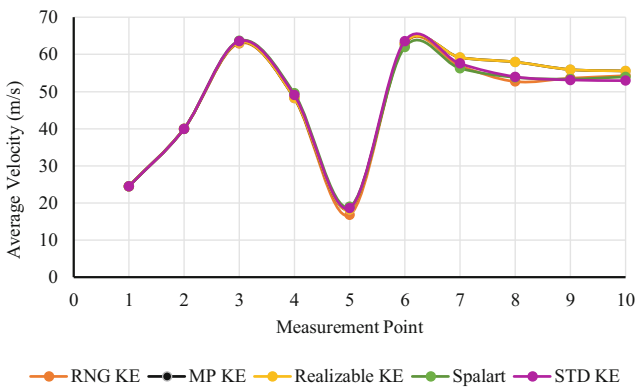

Fig. 6 Comparison of average velocity at ten points for five turbulence models

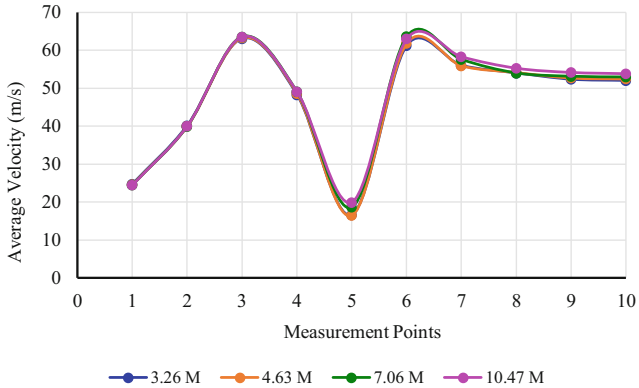

Fig. 7 Comparison of average velocity at ten points for the mesh independence study

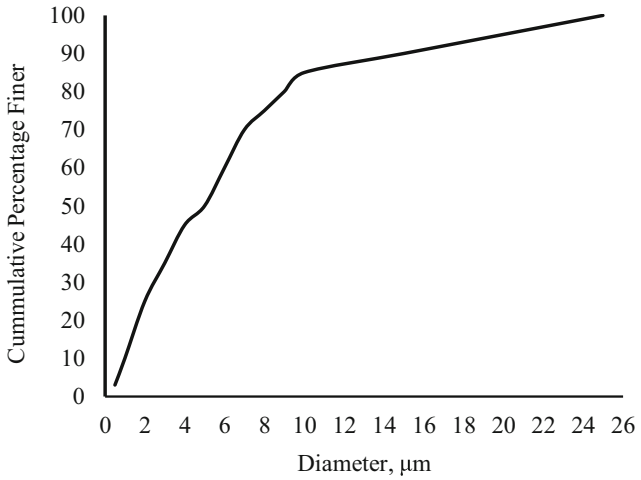

Fig. 8 Cumulative size distribution of continuous miner face dust sample [37]

where C_D is the drag coefficient, V is the relative velocity of fluid and particle, and A is the projected area of the particle. C_D is calculated using the following formula:

$$C_D = \frac{24}{Rep}\left[1 + 0.1255(Rep)^{0.72}\right] \qquad Rep \leq 1000 \qquad (11)$$

$$C_D = 0.44 \qquad Rep > 1000 \qquad (12)$$

$$Rep = \frac{VD_p}{\upsilon} \qquad (13)$$

where υ is the kinematic viscosity of the fluid.

2.4 Mesh Independence Study

An unstructured computational mesh was generated in the computational domain using the finite volume method. The tetrahedral element mesh was created in the computational domain volume using the advancing front method. The wall boundary was refined using three prism layers to capture the effect of walls on the fluid with high numerical accuracy. The Y^+ value at all walls was maintained between 30 and 300 to permit the correct application of logarithmic law wall function, except some low velocity, recirculating zones in the center of the vortex chamber. Mesh refinement was performed in the region of a large gradient of computed variables, whereas a relatively coarser mesh was used in the areas with an insignificant or small variation to save computational time.

To ensure that the results obtained through CFD modeling would not depend on the mesh resolution, and to explain the physics with utmost accuracy, a grid independence study was

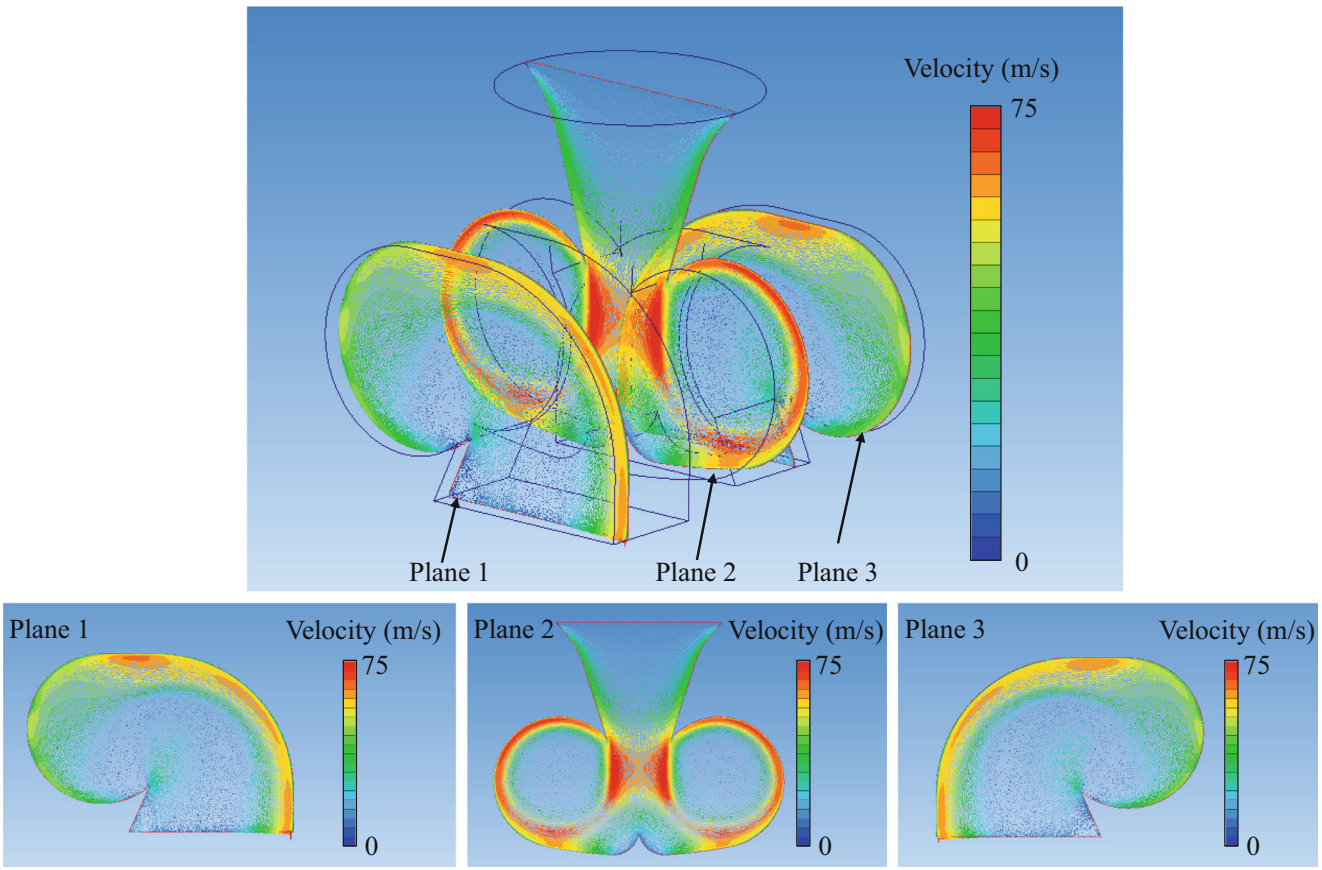

Fig. 9 Velocity vectors on three parallel planes for 12-m/s scrubber inlet velocity

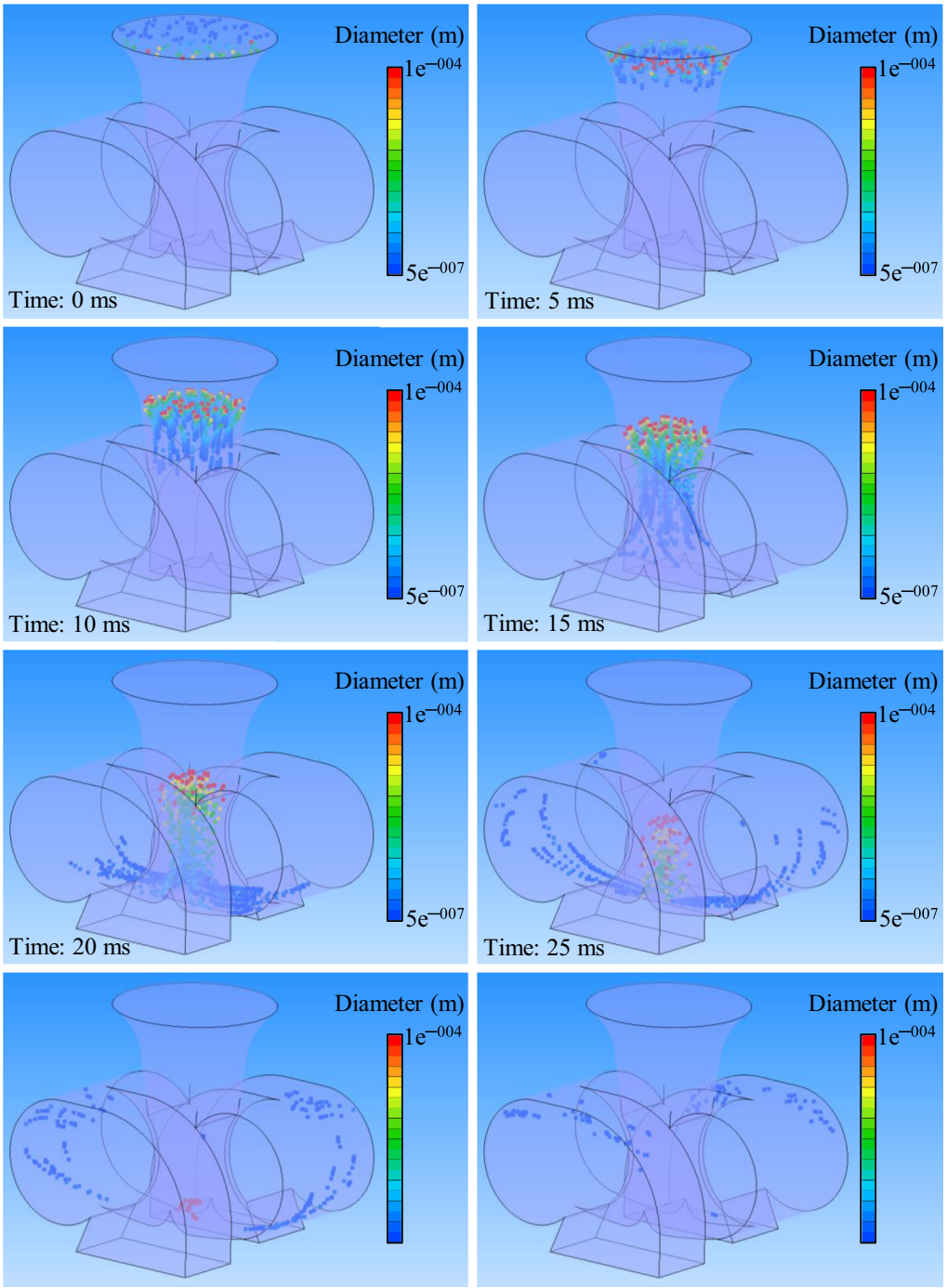

Fig. 10 Status of different diameters particles at various time points for 12-m/s scrubber inlet velocity

carried out. The grid independence study started with a coarse mesh that was gradually refined until the variations in the results were deemed acceptable. Four different cases, with a computational domain element growth factor of approximately 1.5, were tested for the scenario in which the vortecone scrubber was operating at 12.0 m/s inlet velocity. The total numbers of elements in the computational domain for the four cases were 3.26 million, 4.63 million, 7.06 million, and 10.47 million, in that order.

The magnitude of average air velocities was measured and compared on the ten points shown in Fig. 5. Figure 7 shows the mesh independence study results for average velocity at the points marked in Fig. 5. The mesh independence study indicated that results became independent of the grid size at 7.06 million elements. Based on the results obtained from the grid independence study, the CFD validation was performed at 7.06 million elements in the computational domain.

2.5 Analysis Conditions

The standard wall function based on the logarithmic law was applied to predict fluid velocity close to the walls of the computational domain. Air was assumed to be incompressible with density and dynamic viscosity values of 1.206 kg/m^3 and 1.83e^{-5} Pa s, respectively at an ambient temperature of 20 °C. Boundary conditions for the steady-state simulation included the velocity of air going into the conical section of the vortecone and the zero static pressure at the outlet of the duct. The boundary walls were considered to be smooth and stationary.

In the steady state, the solution was assumed to converge when the average residuals of all the variables were less than 10^{-4} within a cycle, and mass flow was balanced. The results of steady-state simulations were used as the initial flow field for transient-state simulation. The time step for the transient analysis was kept very low to achieve a Courant number below 1.0.

Two dust particle size distributions with mass particles of density 1200 kg/m^3 were used: (a) a hypothetical, uniform particle size distribution with particle size varying from 0.5 to 100.0 μm (0.5, 1, 2, 3, 4, 5, 6, 7, 8, 9, 10, 15, 20, 25, 30, 40, 50, 60, 80, and 100 μm) and (b) a measured particle size distribution of dust generated at a continuous miner face. Figure 8 shows the dust particle size distribution obtained from a report published by the U.S. Department of the Interior, Bureau of Mines in 1987 [37]. Five simulations (for five vortecone inlet air velocity conditions) were performed for each dust particle size distribution. A total of 2000 dust particles were released at time zero ($t = 0.00$ s) at the inlet for each simulation. Initially, at $t = 0.00$ s, the particles were considered to have the same velocity as the air. Because the water film introduced at the vortecone inlet flows continuously on the inner wall of the vortecone, and it follows the same path as air, it was assumed that the dust particles that hit the wall of the vortecone were captured by water and hence disappeared from the flow domain. The dust particles that could not be captured by the wall escaped the scrubber and therefore contributed to its overall inefficiency. The escaped dust particles were counted, and the capture efficiency of the vortecone was calculated by dividing the number of particles escaped from the scrubber by the total number of particles introduced in the vortecone.

3 Results and Discussion

Figure 9 presents the velocity contours obtained from the single-phase, steady-state simulation, representing conditions before dust release. As expected, air velocity increases in the conical inlet. A high-velocity, turbulent flow is observed close to the walls of the mixing chamber, vortex chamber, and scrubber discharge, helping promote particle-water interaction. The airflow in the center of the vortex chamber and scrubber discharge is low and recirculating causing power loss.

Results of the CFD simulation for the condition after uniform particle size dust release are presented in Figs. 10 and 11. Figure 10 shows the instantaneous solution of all the dust particles at different times. From the simulation, it is clear that the number of particles in the vortecone decreases as they move downwind from scrubber inlet meaning the particles are captured at the wall of the vortecone. Also, the number of large diameter particles reduces more rapidly than small-diameter particles indicating large particles are more prone to becoming captured. Figure 11 presents the trajectories of dust particles of different diameters in the computational domain. Again, it is clear that the vortecone scrubber operating at an inlet velocity of 12 m/s has a high capture rate for larger particles, and most particles of a diameter greater than 10 μm are captured before reaching the vortex chamber.

3.1 Impact of Inlet Velocity

The study indicates that the cleaning efficiency of the vortecone scrubber increases with inlet velocity, both for uniform and measured particle size distribution, as shown in Fig. 12. Higher inlet velocity creates higher particle momentum in the conical inlet and higher centrifugal force in the vortex chamber, causing more particle-water interaction and therefore more dust capture. Because the uniform particle size distribution has

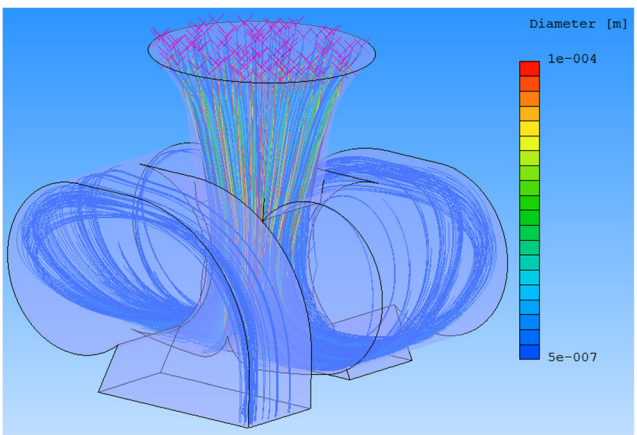

Fig. 11 Trajectories of particles of different diameters in the vortecone for 12-m/s scrubber inlet velocity

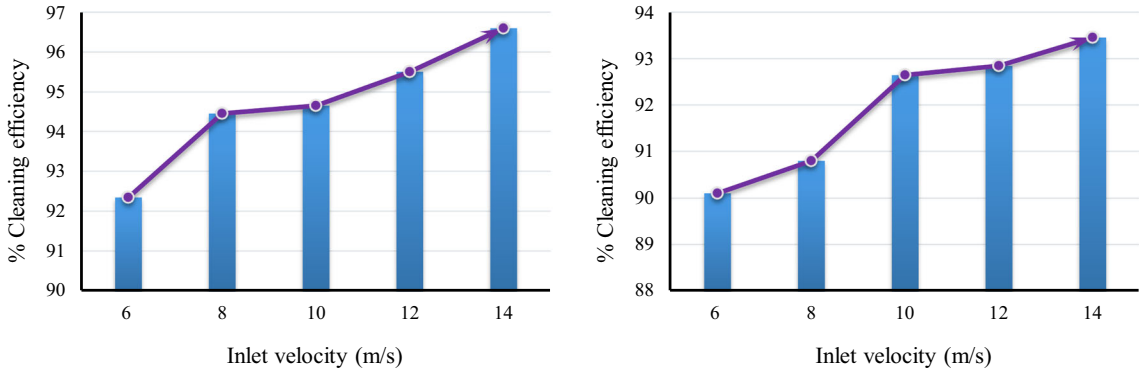

(a) Uniform particle size distribution (b) Measured particle size distribution

Fig. 12 Scrubber cleaning efficiency vs. inlet velocity showing a positive correlation

a higher number of large diameter particles than the measured particle size distribution, the cleaning efficiencies in the uniform particle size distribution cases are slightly higher than those in measured particle size distribution cases.

3.2 Impact of Particle Size

Figure 13 shows the effect of particle size on dust cleaning efficiency of the vortecone scrubber. It verifies the observation made earlier in this section that the cleaning efficiency increases with particle size. A small particle, having low inertia, experiences low momentum in the conical inlet and low centrifugal force in the vortex chamber, and therefore follows the trajectory of the airflow and is more likely to escape the vortecone. From the simulation result, it can be seen that the vortecone can capture approximately 73%, 76%, 80%, 86%, 91%, 96%, and 100% of 0.5-, 1.0-, 2.0-, 3.0-, 4.0-, 5.0-, 6.0-, and 7.0-μm diameter particles, respectively, in both particle size distribution scenarios.

4 Conclusion

A study was carried out to verify the performance of a novel vortecone scrubber for use in capturing dust from the dust-laden air generated at an underground mine face. The ultimate goal was to replace a maintenance-intensive flooded-bed scrubber system with a highly efficient, maintenance-free vortecone scrubber system for use with a continuous miner. Computational fluid dynamics modeling of dust capture through the vortecone was performed for various scrubber inlet velocities ranging from 6 to 14 m/s. The results of this study indicate that the vortecone scrubber system has a higher cleaning efficiency than the flooded-bed scrubber system and that its cleaning efficiency positively correlated to airflow velocity. The vortecone scrubber can capture 90.1% and 93.4% of particles at 6.0- and 14.0-m/s inlet velocities, respectively. Furthermore, the research shows a higher capture rate for larger particles, with 100% of particles of diameter 7 μm and above being captured. Finally, the study indicates a vortecone scrubber can be a better alternative than a flooded-bed scrubber. Because of its reduced maintenance frequency, the vortecone scrubber offers greater system availability and therefore greater production rates.

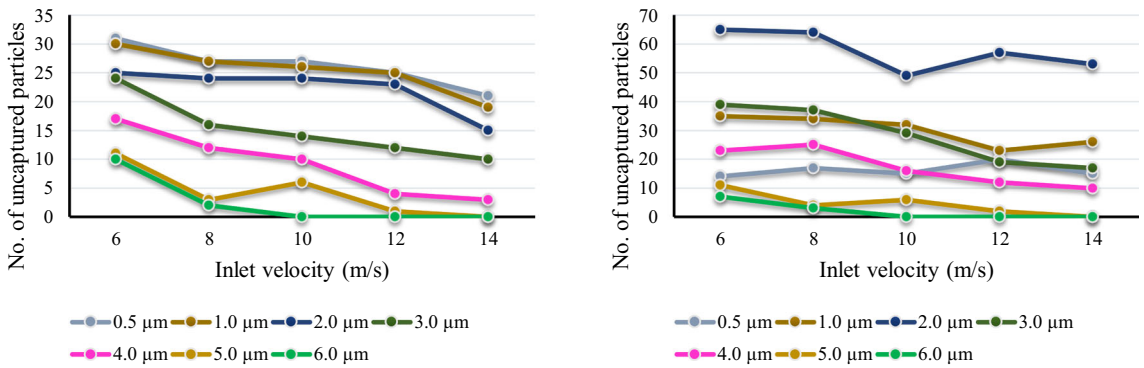

(a) Uniform particle size distribution (b) Measured particle size distribution

Fig. 13 Number of uncaptured particles for different particle diameters

Funding information The funding for this research was provided by the National Institute for Occupational Safety and Health (NIOSH) (grant number 200-2014-59922).

Compliance with Ethical Standards

Conflict of Interest The authors declare that they have no conflict of interest.

References

1. U.S. Department of Labor (2014) Lowering miners' exposure to respirable coal mine dust, including continuous personal dust monitors. In: Fed Regist Vol 79, Number 84. http://arlweb.msha.gov/regs/fedreg/final/2014finl/2014-09084.asp. Accessed 1 May 2014
2. Sinclair J (1958) Environmental conditions in coal mines: including fires, explosions, rescue and recovery work. Pitman
3. NIOSH (2008) Work-related lung disease surveillance report 2007, Volume 1. Dep Heal Hum Serv Centers Dis Control Prev Natl Inst Occup Saf Heal Div Respir Dis Stud DHHS
4. Cashdollar KL, Sapko MJ (2006) Explosion hazards of coal dust in the presence of methane. In: Handbook for methane control in mining, pp 147–150
5. U.S. Department of Labor (2001) Report of investigation, fatal underground coal mine explosions, September 23, 2001, No. 5 Mine, Jim Walter Resources, Brookwood, Tuscaloosa County, Alabama, ID No. 01–01322
6. U.S. Department of Labor (2011) Report of investigation, fatal underground mine explosion, April 5, 2010, Upper Big Branch Mine-South, Performance Coal Company, Montcoal, Raleigh County, West Virginia, ID No. 46–08436
7. U.S. Department of Labour (2009) End Black Lung - ACT NOW. http://arlweb.msha.gov/S&HINFO/BlackLung/homepage2009.asp. Accessed 11 Oct 2016
8. U.S. Department of Labor (2010) Lowering miners' exposure to respirable coal mine dust, including continuous personal dust monitors, proposed rule. In: 30 CFR Parts 70, 71, 72, al. http://arlweb.msha.gov/REGS/FEDREG/PROPOSED/2010PROP/2010-25249.PDF. Accessed 11 Oct 2016
9. U.S. Department of Labor (2014) Final rule. http://arlweb.msha.gov/regs/fedreg/final/2014finl/2014-09084.asp. Accessed 26 August 2015
10. Wang W, Peng FF (1991) Analyses of respirable dust distributions with multiple dust sources on longwall faces. In: Proceedings of Society for Mining, Metallurgy & Exploration. pp 367–375
11. Colinet JF, Spencer ER, Jankowski RA (1997) Status of dust control technology on U.S. longwalls. In: Proceedings of 6th International Mine Ventilation Congress. pp 345–351
12. Arya S, Sottile J, Novak T (2018) Development of a flooded-bed scrubber for removing coal dust at a longwall mining section. Saf Sci 110:204–213. https://doi.org/10.1016/j.ssci.2018.08.003
13. Arya S, Sottile J, Rider JP, Colinet JF, Novak T, Wedding C (2018) Design and experimental evaluation of a flooded-bed dust scrubber integrated into a longwall shearer. Powder Technol 339:487–496. https://doi.org/10.1016/j.powtec.2018.07.072
14. Arya S, Novak T, Saito K et al (2019) Empirical formulae for determining pressure drop across a 20-layer flooded-bed scrubber screen. Min Metall Explor. https://doi.org/10.1007/s42461-019-0091-5
15. Arya S (2018) Investigation of the effectiveness of an integrated flooded-bed dust scrubber on a longwall shearer through laboratory testing and CFD simulation. University of Kentucky
16. Campbell JAL, Moynihan DJ, Roper WD, Willis C (1983) Dust control system and method of operation
17. Wedding WC, Novak T, Arya S, Kumar A (2015) CFD modeling of a flooded-bed scrubber concept for a longwall shearer operating in a U.S. Coal Seam. In: Proceedings of 15th US Mine Ventilation Symposium. pp 385–390
18. Wirch S, Jankowski R (1991) Shearer-mounted scrubbers, are they viable and cost effective. In: Proceedings of 7th US Mine Ventilation Symposium. pp 319–325
19. NIOSH (1997) Hazard identification 1: exposure to silica dust on continuous mining operations using flooded-bed scrubbers. U.S. Department of Health and Human Services, Public Health Service, Centers for Disease Control and Prevention, National Institute for Occupational Safety and Health, DHHS (NIOSH)
20. Colinet JF, Reed WR, Potts JD (2014) Continuous mining dust levels in 20-foot cuts with and without a scrubber operating. In: Proceedings of Society for Mining, Metallurgy & Exploration. Salt Lake City, UT, p Preprint 14–033
21. Colinet JF, Reed WR, Potts JD (2013) Impact on respirable dust levels when operating a flooded-bed scrubber in 20-foot cuts. In: U.S. Department of Health and Human Services, Public Health Service, Centers for Disease Control and Prevention, National Institute for Occupational Safety and Health, DHHS (NIOSH) Publication No. 2014-105, RI 9693. Pittsburgh\
22. Potts JD, Reed WR, Colinet JF (2011) Evaluation of face dust concentrations at mines using deep-cutting practices. In: U.S. Department of Health and Human Services, National Institute for Occupational Safety and Health, DHHS (NIOSH) Publication No. 2011-131, RI 9680. Pittsburgh
23. Salazar AJ, Saito K, Alloo RP, Tanaka N (2000) Wet scrubber and paint spray booth including the wet scrubber
24. Saito K (2008) Progress in Scale Modeling: Summary of the First International Symposium on Scale Modeling (ISSM I in 1988) and Selected Papers from Subsequent Symposia (ISSM II in 1997 through ISSM V in 2006). Springer Netherlands
25. Li T, Salarzar AJ, Saito K (2009) Experimental and numerical feasibility study of modifying automotive wet scrubber for capturing particulate in coal-fired power plants. In: Proceedings of 6th International Symposium on Scale Modeling. Kauai, Hawaii, pp 1–10
26. Kurnia JC, Sasmito AP, Mujumdar AS (2014) Dust dispersion and management in underground mining faces. Int J Min Sci Technol 24:39–44. https://doi.org/10.1016/J.IJMST.2013.12.007
27. Yueze L, Akhtar S, Sasmito AP, Kurnia JC (2017) Prediction of air flow, methane, and coal dust dispersion in a room and pillar mining face. Int J Min Sci Technol 27:657–662. https://doi.org/10.1016/J.IJMST.2017.05.019
28. Geng F, Luo G, Wang Y, Peng Z, Hu S, Zhang T, Chai H (2018) Dust dispersion in a coal roadway driven by a hybrid ventilation system: a numerical study. Process Saf Environ Prot 113:388–400. https://doi.org/10.1016/J.PSEP.2017.11.010
29. Gilmore RC, Marts JA, Brune JF et al (2015) Simplifying CFD modeling of longwall gobs with modular meshing approach. Min Eng 67:2015
30. Hu S, Feng G, Ren X, Xu G, Chang P, Wang Z, Zhang Y, Li Z, Gao Q (2016) Numerical study of gas–solid two-phase flow in a coal roadway after blasting. Adv Powder Technol 27:1607–1617. https://doi.org/10.1016/J.APT.2016.05.024
31. Lolon SA, Brune JF, Bogin GE et al (2017) Computational fluid dynamics simulation on the longwall gob breathing. Int J Min Sci Technol 27:185–189. https://doi.org/10.1016/J.IJMST.2017.01.025
32. Wang Z, Ren T, Ma L, Zhang J (2018) Investigations of ventilation airflow characteristics on a longwall face—a computational approach. Energies 11
33. Zhou G, Zhang Q, Bai R, Fan T, Wang G (2017) The diffusion behavior law of respirable dust at fully mechanized caving face in

coal mine: CFD numerical simulation and engineering application. Process Saf Environ Prot 106:117–128. https://doi.org/10.1016/J.PSEP.2016.12.005

34. Fig MK, Bogin GE, Brune JF, Grubb JW (2016) Experimental and numerical investigation of methane ignition and flame propagation in cylindrical tubes ranging from 5 to 71 cm – part I: effects of scaling from laboratory to large-scale field studies. J Loss Prev Process Ind 41:241–251. https://doi.org/10.1016/j.jlp.2016.03.018
35. Ajayi K, Shahbazi K, Tukkaraja P, Katzenstein K (2019) Numerical investigation of the effectiveness of radon control measures in cave mines. Int J Min Sci Technol 29:469–475. https://doi.org/10.1016/J.IJMST.2018.07.006
36. Software Cradle Co. Ltd. (2015) User's Guide Basics of CFD Analysis
37. Ramani R V, Mutmansky JM, Bhaskar R, Qin J (1987) Fundamental studies on the relationship between quartz levels in the host material and the respirable dust generated during mining, volume 1: experiments, results and analysis. Washington, DC